CHEM**MED**CHEM

CHEMISTRY ENABLING DRUG DISCOVERY

Accepted Article

Title: Asymmetric Disulfanylbenzamides as Irreversible and Selective Inhibitors of Staphylococcus aureus Sortase A

Authors: Fabian Barthels, Gabriella Marincola, Tessa Marciniak, Matthias Konhäuser, Stefan Hammerschmidt, Jan Bierlmeier, Ute Distler, Peter R. Wich, Stefan Tenzer, Dirk Schwarzer, Wilma Ziebuhr, and Tanja Schirmeister

FULL PAPER

Asymmetric Disulfanylbenzamides as Irreversible and Selective Inhibitors of *Staphylococcus aureus* Sortase A

Fabian Barthels[a], Gabriella Marincola[b], Tessa Marciniak [b], Matthias Konhäuser[a], Stefan Hammerschmidt[a], Jan Bierlmeier[c], Ute Distler[d,e], Peter R. Wich[a,f], Stefan Tenzer[d], Dirk Schwarzer[c], Wilma Ziebuhr[b], Tanja Schirmeister*[a]

[a]   F. Barthels (ORCID 0000-0001-7950-2158), M. Konhäuser, S. Hammerschmidt, Jun.-Prof. Dr. P. R. Wich (ORCID 0000-0003-1522-0340), Prof. Dr. T. Schirmeister (ORCID 0000-0002-4587-5076)
      Institute for Pharmacy and Biochemistry
      Johannes-Gutenberg-University of Mainz
      Staudinger Weg 5, 55128 Mainz, Germany
      E-mail: schirmei@uni-mainz.de
[b]   Dr. G. Marincola (ORCID 0000-0001-9227-6554), T. Marciniak, Dr. W. Ziebuhr (ORCID 0000-0002-7059-1614)
      Institute for Molecular Infection Biology
      Julius-Maximilians-University of Würzburg
      Josef-Schneider-Strasse 2, 97080 Würzburg, Germany
[c]   J. Bierlmeier (ORCID 0000-0002-7261-4744), Prof. Dr. D. Schwarzer (ORCID 0000-0002-7477-3319)
      Interfaculty Institute of Biochemistry
      Eberhard-Karls-University of Tübingen
      Hoppe-Seyler-Strasse 4, 72076 Tübingen, Germany
[d]   Dr. U. Distler (ORCID 0000-0002-8031-6384), Prof. Dr. S. Tenzer (ORCID 0000-0003-3034-0017)
      Institute for Immunology, University Medical Center
      Johannes-Gutenberg-University of Mainz
      Langenbeckstr. 1, 55131 Mainz, Germany
[e]   Dr. U. Distler (ORCID 0000-0002-8031-6384)
      Focus Program Translational Neuroscience (FTN), University Medical Center
      Langenbeckstr. 1, 55131 Mainz, Germany
[f]   Jun.-Prof. Dr. P. R. Wich (ORCID 0000-0003-1522-0340)
      School of Chemical Engineering
      University of New South Wales
      Science and Engineering Building, Sydney, NSW 2052, Australia

      Supporting information for this article is given via a link at the end of the document.

Abstract: *Staphylococcus aureus* is one of the most frequent causes of nosocomial and community-acquired infections responsible for ten-thousands of deaths per year by drug-resistant strains. *S. aureus* sortase A inhibitors are designed to interfere with virulence determinants. We identified disulfanylbenzamides as a new class of potent inhibitors against sortase A acting by covalent modification of the active site cysteine. A broad series of derivatives were synthesized to derive structure-activity-relationship (SAR). *In vitro* and *in silico* methods allowed rationalizing the experimentally observed binding affinities and selectivities. The most active compounds were found to have single-digit micromolar K_i values and showed up to 66% reduction of *S. aureus* fibrinogen attachment at an effective inhibitor concentration of 10 µM. This new molecule class exhibited minimal cytotoxicity, low bacterial growth inhibition and impaired sortase-mediated adherence of *S. aureus* cells.

Introduction

The ongoing spread of antibiotic resistance among Gram-positive bacteria such as *Staphylococcus aureus* highlights the need for new treatment options beyond traditional antibiotics. In this respect, exploring virulence mechanisms as drug targets might provide novel opportunities to interfere with bacterial pathogenicity.[1] The cysteine transpeptidase sortase A (SrtA) was considered as a putative anti-virulence drug target, which may be

addressed also in combination with classical antibiotics' target structures.[2] SrtA mediates the attachment of surface proteins to the bacterial cell wall and it was shown that an *S. aureus* ΔSrtA mutant is clearly attenuated in mouse infection models compared to the wildtype.[3,4] SrtA inhibitors are likely to interfere with adherence and intercellular communication rather than with bacterial growth, thus imposing a lower selective pressure to promote resistance development.[5] Since neither genetic deletion[6] nor selective chemical inhibition[7–9] of *S. aureus* SrtA was found to cause cytotoxic or growth inhibitory effects on bacterial cells, the enzyme meets the requirements of an anti-virulence target. Microbial surface components recognizing adhesive matrix molecules (MSCRAMMs) are bacterial surface proteins utilized during pathogenesis for adherence to endothelial host cells and playing a role in immune evasion.[10] Many of these virulence-associated proteins are secreted as precursors with C-terminal LPXTG-tagged sorting-signals. At the bacterial cell wall, they are recognized and cleaved between threonine and glycine by the membrane-anchored transpeptidase SrtA.[11] Subsequent ligation to the pentaglycine tail of the peptidoglycan layer yields the covalent attachment to the bacterial outer surface.[12] In *S. aureus*, approximately 20 surface proteins have been identified as naturally occurring SrtA substrates, including several factors that are involved in pathogenicity, such as protein A (SpA), fibronectin-binding proteins (FnbpA/B), clumping factors (ClfA/B), serine-aspartic acid repeat proteins (SdrC/D/E) and staphylococcal surface proteins (Sas).[13,14]

FULL PAPER

The eight-stranded β-barrel protein SrtA possesses three conserved residues within the sortase family: His62, Cys126, and Arg139, each of which cannot be mutated without disrupting enzymatic functionality.[15] Structural similarities between the transpeptidase SrtA and the papain protease were noticed[16], however, enzymatic characteristics of the *S. aureus* SrtA differ significantly from most proteases: (i) The catalytic Cys126 is "reversely protonated", which means it does not form a thiolate-imidazolium pair, and thus, only a small fraction (<0.1%) of SrtA is competent for catalysis at physiological pH 7.4.[17] (ii) The active site is predominantly defined by the intrinsic flexibility of the β6/7- and β7/8-loops.[18] (iii) The most active form of SrtA is constituted as a homo-dimer with a K_D=55 μM.[19] (iv) The K_M values for both, the LPXTG- and Gly$_n$-substrates are exceptionally high (K_M= 5.5 mM and 0.14 mM), probably due to the fact that the enzyme and both substrates are spatially co-localized at the outer membrane yielding high local concentrations.[20] (v) The high redox potential of the catalytic Cys126 (1.27 V) makes SrtA insensitive towards oxidation stress contributing to *S. aureus* phagocytotic survival.[21]

Previous research campaigns investigated competitive-reversible *S. aureus* SrtA inhibitors including promising scaffolds such as 2-morpholinobenzoates[22], thiadiazoles[7,23], 2-phenylthiazoles[24], macrocyclic peptides[25], 2-phenylbenzoxazoles[26], and various other inhibitors.[8,27,28] However, the most active compounds were found to be irreversible covalent inhibitors containing an electrophilic warhead that reacts with the active-site Cys126 of SrtA.[29–33] While having significant inhibition in the low micromolar range, they typically exhibit poor target selectivity or are cytotoxic such as quinones[34], rhodanines[30] or benzisothiazolinones[32]. Zhulenkovs *et al.* solved the NMR-structure of SrtA in complex with a covalent benzisothiazolinone adduct. Reaction with the active site Cys126 occurred via ring-opening of the isothiazolinone moiety yielding a covalent disulfide bond (Fig 1A).
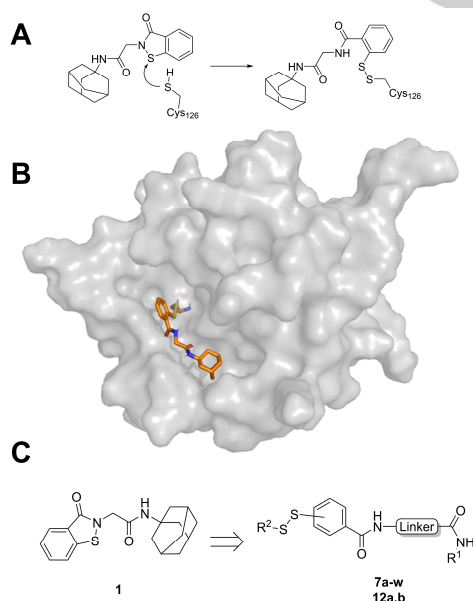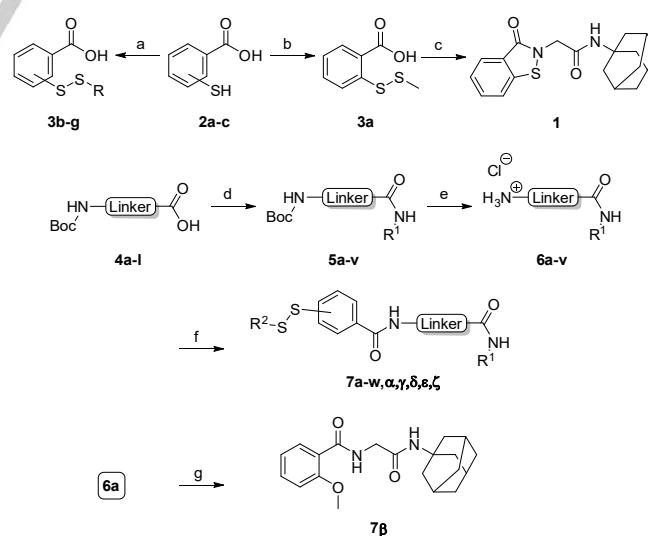
In the corresponding NMR-structure (pdb: 2MLM), the ligand displayed a reasonable fit, mimicking substrate binding in the active-site pocket (Fig 1B). Asymmetric disulfides are known inhibitors of cysteine proteases[35–37], thus, we decided to investigate a disulfide warhead chemotype exchange and systematic scaffold optimization to generate more selective and less cytotoxic disulfide-based SrtA inhibitors (Fig 1C).

Results and Discussion

Synthesis of the inhibitors

Disulfanylbenzamides were synthesized based on a known procedure for asymmetric disulfides (Scheme 1).[38] Commercially available sulfanylbenzoic acids **2a–c** were activated at −50 °C with trichloroisocyanuric acid (TCCA) to form electrophilic sulfenyl chlorides *in situ*. The subsequent conversion with nucleophilic alkyl thiols provided the disulfanylbenzoic acids **3b–g**. Since methyl mercaptan is gaseous at room temperature, for 2-(methyldisulfanyl)benzoic acid **3a** a different strategy was employed. *S*-methyl methanethiosulfonate as thiomethyl-transferring reagent was utilized to convert thiosalicylic acid **2a** to 2-(methyldisulfanyl)benzoic acid **3a**.[39] Boc-protected amino acids **4a–l** were coupled to various aromatic and aliphatic amines (R^1) in the presence of 2-(1*H*-benzotriazole-1-yl)-1,1,3,3-tetramethylaminium tetrafluoroborate (TBTU) to provide the inhibitor scaffold precursors **5a–v**. The deprotection of the Boc-group was achieved by treatment with hydrochloric acid. Finally, the disulfanylbenzoic acids **3a–g** were coupled in the presence of TBTU with the appropriate amine hydrochlorides **6a–v** to provide the desired test compounds **7a–w** and **7α–ζ** (Scheme 1). Parent compound **1** was prepared in a one-pot procedure from **3a** and **6a**. Both reactants were coupled by means of TBTU. The subsequent treatment with lithium hydroxide at 60 °C yielded the elimination of methyl mercaptan and provided the benzisothiazolinone inhibitor **1**.[40]

Figure 1. A) The reaction of benzisothiazolinones with the active site Cys126 in *S. aureus* SrtA. B) NMR-structure of the benzisothiazolinone inhibitor (**1**) covalently bound to *S. aureus* SrtA (pdb: 2MLM). C) Warhead chemotype exchange and scaffold-hopping strategy to transform the literature-known inhibitor (**1**) to disulfanylbenzamides (**7a–w** and **12a,b**).[32]

Scheme 1. a) Trichloroisocyanuric acid, R-SH, ACN, −50 °C to rt, 15 min; 56–69%; b) *S*-methyl methanethiosulfonate, MeOH, rt, 16 h, 86%; c) (i) **6a**, TBTU, DIPEA, DMF, rt, 16 h (ii) 4M LiOH$_{aq}$, 60 °C, 4 h, 75%; d) R^1-NH$_2$, TBTU, DIPEA, EtOAc, rt, 72 h, 24–96%; e) 12M HCl$_{aq}$/THF (1:1), rt, 1 h, 74–99%; f) R^2-SS-PhCOOH, TBTU, DIPEA, EtOAc, rt, 16 h, 23–89%; g) *o*-anisic acid, TBTU, DIPEA, EtOAc, rt, 72 h, 82%.

2

FULL PAPER

For the synthesis of the aspartic acid-based inhibitors **12a,b** a different protection group strategy was used (Scheme 2). Briefly, the Cbz/*t*Bu-protected aspartic acid derivates **8a,b** were coupled by means of TBTU to yield the amides **9a,b**. The deprotection of the N-terminal Cbz-group was achieved by Pd-catalyzed hydrogenolysis to yield the amines **10a,b**. The disulfanylbenzoic acids **3a** or **3d** were coupled to the appropriate amines in the presence of TBTU yielding the inhibitor scaffold precursors **11a,b**. Finally, the deprotection of the *tert*-butyl ester with trifluoroacetic acid yielded the compounds **12a,b**.
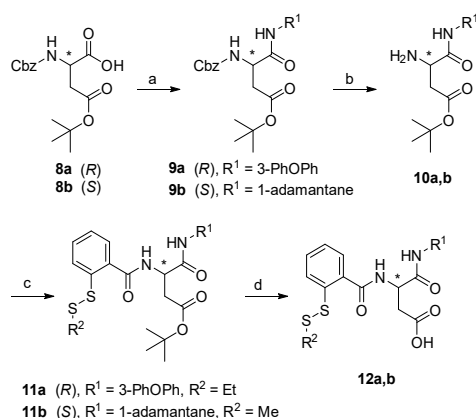
Scheme 2. a) R^1-NH$_2$, TBTU, DIPEA, EtOAc, rt, 72 h, 68–96%; b) H$_2$ (60 psi), Pd/C, MeOH, rt, 16 h, 92–99%; c) R^2-SS-PhCOOH, TBTU, DIPEA, EtOAc, rt, 16 h, 79–83%; d) TFA/DCM, rt, 2 h, 91–99%.

Substrate-based diacyl hydrazide inhibitors (**16a,b**) were synthesized starting from proline benzyl ester **13** and Boc-leucine to yield the dipeptide ester **14**. Hydrazinolysis of the benzyl ester gave the hydrazide **15**, which was either TBTU-coupled with **3a** to yield the disulfanylbenzamide **16a** or converted with maleic anhydride to the mono-maleamide **16b** (Scheme 3).
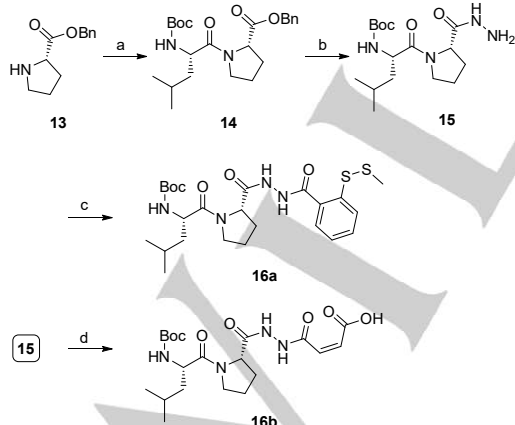
Scheme 3. a) Boc-Leu-OH, TBTU, DIPEA, EtOAc, rt, 72 h, 56%; b) Hydrazine hydrate, MeOH, rt, 16 h, 74%; c) **3a**, TBTU, DIPEA, EtOAc, rt, 16 h, 16%; d) Maleic anhydride, AcOH, rt, 16 h, 79%.

Irreversible inhibition of *S. aureus* sortase A

To evaluate the inhibition potency of the compounds, these were tested by means of a fluorometric enzyme assay with

recombinantly expressed *S. aureus* SrtA[41] and Abz-LPETG-Dap(Dnp)-OH as substrate. The inhibitors **7a–w** and **12a,b** were found to act as time-dependent and irreversible inhibitors. Exemplarily, the substrate conversion plot in the presence of inhibitor **12a** is showing the time-dependency of inhibition (Fig 2). The apparent first-order rate constant (k_{obs}) varied hyperbolically with the concentration of the inhibitor. A limiting value was approached asymptotically at higher inhibitor concentrations indicating two-step mechanism kinetics for all inhibitors except for the fragment-like inhibitor **3a** (K_i=367 µM). Benzisothiazolinone **1** was used as a reference inhibitor with a literature reported IC$_{50}$=6.11 µM.[32] For time-dependent inhibitors, reporting IC$_{50}$ values is less suitable since the IC$_{50}$ is strongly depending on the incubation time of enzyme and inhibitor. Moreover, the IC$_{50}$ is depending on the substrate used for the enzyme assays, its K_M value and its concentration.[42] Therefore, we determined the maximum inactivation rate k_{inact}, the dissociation constant of the reversible enzyme-inhibitor complex K_i, and the second-order rate of inhibition k_{2nd}. For compound **1** a k_{inact}=0.0307 s^{-1} was found, which is quite high compared to other targeted covalent inhibitors,[43,44] but gives reason to its bactericidal effects[32] and the unspecific cysteine labeling by benzisothiazolinones.[45]
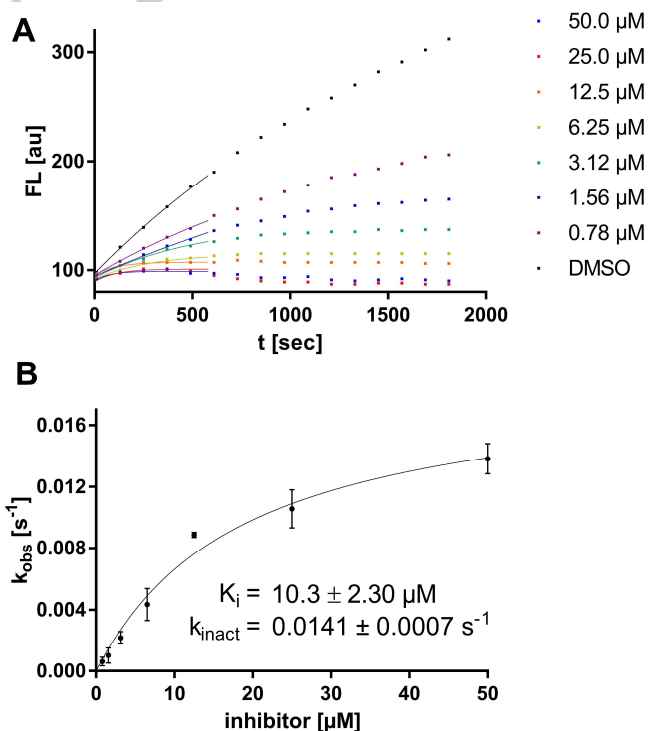

Figure 2. A) Fluorometric assay with compound **12a** showing time-dependent enzyme inhibition with hyperbolic substrate conversion plots in the presence of **12a**. The fluorescence was recorded for 30 min every 30 s. For clarity, only every fourth data point is shown. Lines represent non-linear fits for t<10 min. A magnification plot of the crucial initial phase can be found in SI figure 8. B) k_{obs} vs. [I] for the determination of inhibition constants (K_i, k_{inact}).
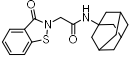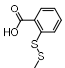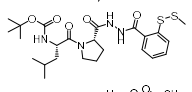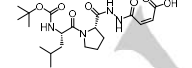
To date, only a few studies characterized irreversible SrtA inhibitors by their inactivation kinetics.[31,46,47] Most of these inhibitors contained the LPAT sorting-signals but utilized different electrophilic warheads (diazoketone, chloroketone or vinyl sulfone). Compared to the parent compound **1**, these warheads

3

FULL PAPER

were 150–5000-fold less reactive (k_{inact}=0.0002 s^{-1}–6.6·10^{-6} s^{-1}), however, the vinyl sulfone was shown to gain significant reactivity above pH 8.00 due to the deprotonation of Cys126 (pK$_a$=9.4[48]). Since the peptidoglycan is slightly acidic[49] and several Gram-positive bacteria have trained themselves by evolution for survival in low-pH environment,[50] we raised the hypothesis that inhibitors with an optimum effect at pH 8.00 or above are unsuitable to target SrtA *in cellulo*. To investigate the pH-dependence of the novel disulfanylbenzamide warhead in comparison to a common Michael-acceptor warhead, we designed sorting-signal derived leucine-proline dipeptide inhibitors, with disulfanylbenzamide (**16a**) and mono-maleamide (**16b**) warheads and characterized their inhibition kinetics and pH-dependence as presented in table 1 and figure 3.

Disulfanylbenzamide inhibitor **16a** showed irreversible inhibition, with a twofold increased affinity compared to the parent compound **1** (K$_i$: 34.2 vs. 16.6 μM), but its overall inhibition potency (k$_{2nd}$) was threefold lower, mainly due to its reduced inactivation rate constant (k$_{inact}$=0.0044 s^{-1}). The dipeptide mono-maleamide **16b** did not show significant inhibition in the standard fluorometric assay, but a two-hour pre-incubation of the enzyme and inhibitor prior to substrate addition led to an IC$_{50}$=20.4 μM. We hypothesized a covalent inhibition mode of **16b** with very slow inactivation kinetics due to the poor nucleophilicity of Cys126. We measured the pH-dependence of SrtA inactivation by **16a** and **16b** at eight different pH-values (6.75–8.50). As shown in figure 3, the general enzymatic activity increased with higher pH-values, which is in coherence with the reported enzyme optimum at pH 8.80.[51] The inhibition potency of the mono-maleamide **16b** was overall low but increased significantly above pH 8.00 either due to the deprotonation of the Cys126 or *in situ* conversion of **16b** to a more electrophilic maleic isoimide, maleimide or pyridazinedione.[52–54]

completely reversible by the addition of 1 mM reducing agents such as DTT or TCEP. Thus, we postulate that covalent targeting of the SrtA Cys126 under physiological conditions was much more effective by disulfanylbenzamides and should be optimized for potency and selectivity (see next chapter).
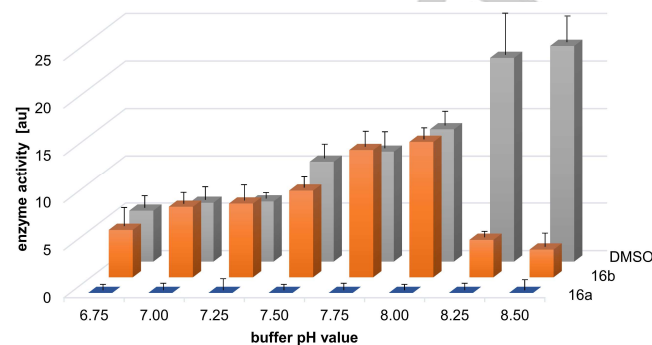

Figure 3. pH-dependency on the inhibition potency of the disulfide inhibitor **16a** and the mono-maleamide inhibitor **16b** at a final inhibitor concentration of 20 μM. The residual enzymatic activity was assessed from the initial slope of the substrate conversion plots. For the inhibitors, no preincubation was used. All results include the mean value and standard deviations from triplicate measurements.

Structure-activity relationship

A broad series of disulfanylbenzamides was synthesized to derive structure-activity-relationship (SAR). In fact, 26 out of 32 analogs (**7a–w**, **12a,b** and **16a**) did inhibit SrtA in the fluorometric enzyme assay, but with varying potency. Based on the k$_{2nd}$ values, eight compounds (**12a**, **7a–g**) appeared to be more potent than parent compound **1**, while all investigated disulfanylbenzamides exhibited at least twofold reduced k$_{inact}$ values ranging from 0.0013 s^{-1} to 0.0174 s^{-1} (Table 2). Strikingly, we observed a drop in SrtA inhibition for most modifications on the glycine amino acid linker. This finding suggested that substitution at this position is not well tolerated, except for (*R*)-aspartic acid in inhibitor **12a**, which we hypothesized to interact with Arg139 (Fig 6). Considering the k$_{2nd}$ value, **12a** was the most potent irreversible inhibitor (82,136 M^{-1}min^{-1}). Compounds **7α–ζ** were found to be non-binders displaying <30% inhibition at 50 μM. Interestingly, the (*R*)-phenylalanine derivate **7p** which showed one of the highest binding affinities (K$_i$=2.72 μM) had very low inactivation kinetics (k$_{inact}$=0.0013 s^{-1}). The (*S*)-phenylalanine enantiomer **7γ**, however, did not show any inhibition. No significant loss in activity was observed upon amide-methylation of glycine (**7f**) to sarcosine (**7h**), demonstrating that the activity is not mediated by an *in situ* activation to benzisothiazolinones. More pronounced effects could be associated with the replacement of the amide substituent (R^1), but no clear structural trend was identified. It should be noted that the two most potent compounds identified here (**12a**, **7a**) incorporated a 3-phenoxyaniline substituent (R^1). Intriguingly, the change of the disulfide warhead (R^2) affected both, affinity (K$_i$) and reactivity (k$_{inact}$). The *ortho*-configuration (**7f**) seemed to be strongly preferred over *meta* (**7u**) and *para* (**7α**). The alkyl group (R^2) followed the trend: Me~Et>*i*Pr~*t*Bu>EtPh. A methyldisulfanyl-(**7e**) to methoxy- (**7β**) exchange led to a complete loss of inhibition. We concluded from these findings that both, the warhead's positioning and the steric demand were likely to influence the inhibitor's potency.

Table 1. Inhibition constants (K$_i$, k$_{inact}$, k$_{2nd}$) of the compounds **1**, **3a** and **16a,b** for *S. aureus* SrtA.

Cpd.	structure	K$_i$ [μM]	k$_{inact}$ [s^{-1}]	k$_{2nd}$ [M^{-1}min^{-1}]
1		34.2 ±5.87	0.0307 ±0.0016	53,860 ±6,665
3a		367 ±24.4	0.0072 ±0.0012	1,177 ±119
16a		16.6 ±2.88	0.0044 ±0.0003	15,904 ±1,735
16b		IC$_{50}$=20.4±1.30 μM[a]		

[a] Two-hour preincubation of the enzyme with inhibitor at pH 7.50. All results include the mean value and standard deviations from triplicate measurements.

In contrast, the disulfide inhibitor **16a** showed strong and pH-independent inhibition, indicating that either a negatively charged thiolate as a nucleophile is not required for the reaction with disulfanylbenzamides or that an inhibitor binding-induced zwitterion formation might occur.[55] Besides the classical S$_N$2-mechanism involving a thiolate,[56] thiol-disulfide conversion was reported to proceed via oxidative and radical-mediated pathways, which might be relevant for the action of disulfanylbenzamides on SrtA.[57–60] We could also show the inhibition by **16a** was

FULL PAPER

Table 2. Inhibition constant values (K_i k_{inact}, k_{2nd}) of the compounds **7a–ζ** and **12a,b** for *S. aureus* SrtA.
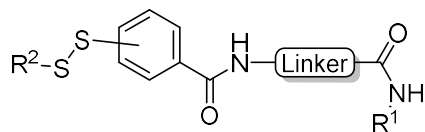
Cpd.	R¹	HN-linker-C(=O)	R²	K_i [μM]	k_{inact} [s⁻¹]	k_{2nd} [M⁻¹min⁻¹]
12a	3-PhOPh	(*R*)-aspartic acid	Et (*ortho*)	10.3±2.30	0.0141±0.0007	82,136±15,136
7a	3-PhOPh	glycine	Et (*ortho*)	11.1±2.15	0.0134±0.0009	72,432±9,581
7b	1-cyclohexanemethyl	glycine	Et (*ortho*)	12.6±2.34	0.0151±0.0010	71,339±8,765
7c	*N,N*-dicyclohexyl	glycine	Et (*ortho*)	8.32±1.31	0.0094±0.0005	63,873±6,238
7d	4-fluorophenyl	glycine	Et (*ortho*)	12.7±2.73	0.0130±0.0010	61,417±8,957
7e	1-adamantyl	glycine	Me (*ortho*)	16.2±2.87	0.0160±0.0012	59,259±6,283
7f	1-adamantyl	glycine	Et (*ortho*)	14.3±2.87	0.0138±0.0011	57,902±7,348
7g	1-adamantyl	(*S*)-proline	Me (*ortho*)	17.0±3.04	0.0163±0.0012	57,529±6,285
7h	1-adamantyl	sarcosine	Et (*ortho*)	20.5±3.53	0.0174±0.0013	50,927±5,414
7i	4-cyclohexanephenyl	glycine	Et (*ortho*)	1.88±0.32	0.0013±0.0001	41,489±4,005
7j	1-napthyl	glycine	Et (*ortho*)	10.0±1.87	0.0066±0.0004	39,600±5,217
7k	1-(thiophene-2-methyl)	glycine	Et (*ortho*)	10.9±1.91	0.0068±0.0004	37,431±4,518
7l	2-adamantyl	glycine	Et (*ortho*)	14.4±2.31	0.0089±0.0005	37,083±3,985
7m	1-adamantyl	glycine	*t*Bu (*ortho*)	6.40±0.84	0.0039±0.0002	36,563±2,984
7n	isobutyl	glycine	Et (*ortho*)	13.5±3.47	0.0082±0.0011	36,444±4,848
7o	1-adamantyl	glycine	*i*Pr (*ortho*)	8.24±1.12	0.0044±0.0002	32,039±2,962
7p	1-adamantyl	(*R*)-phenylalanine	Et (*ortho*)	2.72±0.43	0.0013±0.0001	28,676±2,397
7q	1-adamantyl	β-alanine	Et (*ortho*)	9.60±1.93	0.0028±0.0002	17,500±2,380
7r	1-adamantyl	(*R*)-proline	Et (*ortho*)	5.37±0.83	0.0015±0.0001	16,760±1,515
7s	1-adamantyl	glycine	EtPh (*ortho*)	21.6±3.75	0.0059±0.0005	16,389±1,509
7t	1-adamantyl	isonipecotic acid	Et (*ortho*)	11.0±2.05	0.0026±0.0001	14,182±2,186
12b	1-adamantyl	(*S*)-aspartic acid	Me (*ortho*)	40.2±8.73	0.0092±0.0011	13,731±1,418
7u	1-adamantyl	glycine	Et (*meta*)	24.1±5.94	0.0031±0.0003	7,718±1,242
7v	1-adamantyl	(*S*)-asparagine	Et (*ortho*)	25.3±5.81	0.0029±0.0003	6,877±924
7w	1-adamantyl	(*S*)-alanine	Et (*ortho*)	13.8±3.68	0.0014±0.0001	6,087±1,294
7α	1-adamantyl	glycine	Et (*para*)	n.d.	n.d.	n.d.
7β	1-adamantyl	glycine	see Scheme 1	n.d.	n.d.	n.d.
7γ	1-adamantyl	(*S*)-phenylalanine	Et (*ortho*)	n.d.	n.d.	n.d.
7δ	2-phenylethyl	glycine	Et (*ortho*)	n.d.	n.d.	n.d.
7ε	1-adamantyl	(*R*)-leucine	Et (*ortho*)	n.d.	n.d.	n.d.
7ζ	1-adamantyl	(*S*)-terleucine	Et (*ortho*)	n.d.	n.d.	n.d.

n.d.= <30% inhibition after 30 min at 50 μM of final compound concentration. All results include the mean value and standard deviations from triplicate measurements.

5

FULL PAPER

Characterization of covalent protein adducts

For asymmetric disulfanylbenzamides, two covalent protein adducts are principally possible: the transfer of a thioethyl fragment (+60.0 Da) or the transfer of the thiosalicylamide subunit (+356.2 Da). By using mass spectrometry, we aimed to determine the mode of inhibitor action (Fig 4). The site-specific modification of Cys126 was investigated using trypsin digestion and followed by LC-MS/MS analysis of the tryptic peptides. Three samples were analyzed: the native SrtA and the inhibitor-labeled protein either with **7h** or with **16b**.

For labeling with disulfanylbenzamide **7h**, the measurement was in agreement with the predicted tryptic peptide QLTLITC(SS-Et)DDYNEK (m/z 808.41), encompassing a thioethylated Cys126 (Fig 4A). MS/MS fragmentation confirmed the correct peptide sequence (SI Fig 3). In contrast, the untreated protein sample was lacking this type of modification (Fig 4B). The transfer of a thioethyl fragment (+60.0 Da) seems to be the predominant mode of action, but minor modifications with the thiosalicylamide subunit (+356.2 Da) cannot be completely excluded since corresponding adducts may be below the detection limit or show poor ionization. Thiosalicylamide-protein adducts from benzisothiazolinones were previously linked to haptenization and allergic contact dermatitis[61,62], thus, we evaluate the absence of this adduct form as potentially beneficial. The MS/MS analysis for the mono-maleamide inhibitor **16b** (SI Fig 2) indicated that the inhibition became irreversible due to slow covalent modification of the Cys126 even at physiological pH. However, from labeling with 400 µM inhibitor, we observed only 27% modified peptide masses, supporting the fluorometric assay results (Fig 3), which showed that this reaction is not very efficient at pH 7.50.
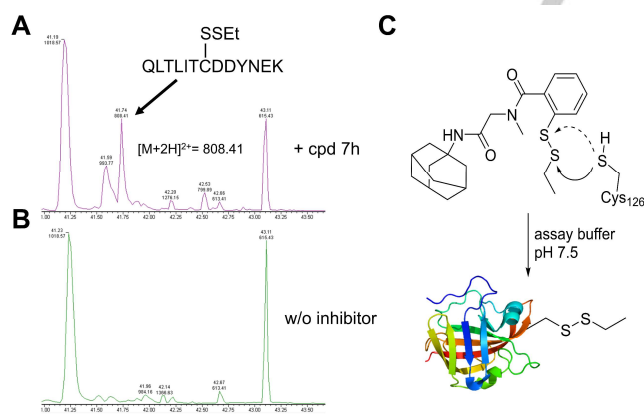

Figure 4. Mass spectrometric analysis of SrtA labeled with compound **7h** revealed the mode of inhibition for disulfanylbenzamides. A) TIC chromatogram of the labeled SrtA showed the distinct modification of the active site Cys126. The peak at m/z=808.41 in the TIC chromatogram (R$_t$=41.7 min) corresponds to the thioethylated peptide QLTLITC(SS-Et)DDYNEK. B) Native SrtA did not show the modification. C) The predominant mode of SrtA inhibition was the transfer of the thioethyl-fragment to Cys126.

In addition to the mass spectrometric analysis, differential scanning fluorimetry (DSF) was used to characterize covalently labeled SrtA proteins (Fig 5A).[63] The native SrtA unfolding temperature was determined to be 50.5 °C in absence of any ligand. By reaction with the benzisothiazolinone compound **1**, the equilibrium was pulled toward the unfolded complex and the

protein was destabilized to a lower melting point (47.1 °C). This agreed with the previously solved NMR-structure (pdb: 2MLM) showing a higher degree of disorder upon covalent complex formation (RMSD$_{mean}$: 1.57 Å vs 3.12 Å; Fig 5B). From a thermodynamic point of view, the loss of the most energetically favorable fold might be compensated here by the released enthalpy of the warhead reaction.

Treatment of sortases with *S*-alkyl methanethiosulfonates led to the quantitative formation of thioalkylated sortase proteins.[64,65] Labeling of SrtA with *S*-ethyl methanethiosulfonate (EMTS) was performed to generate a purely thioethylated SrtA protein, which was found to melt slightly higher than the native SrtA protein (52.7 °C). The protein melt analysis of **7h**-labeled SrtA showed a similar melting point (52.4 °C), thus, these results are strengthening the hypothesis of a thioethyl-fragment transfer.
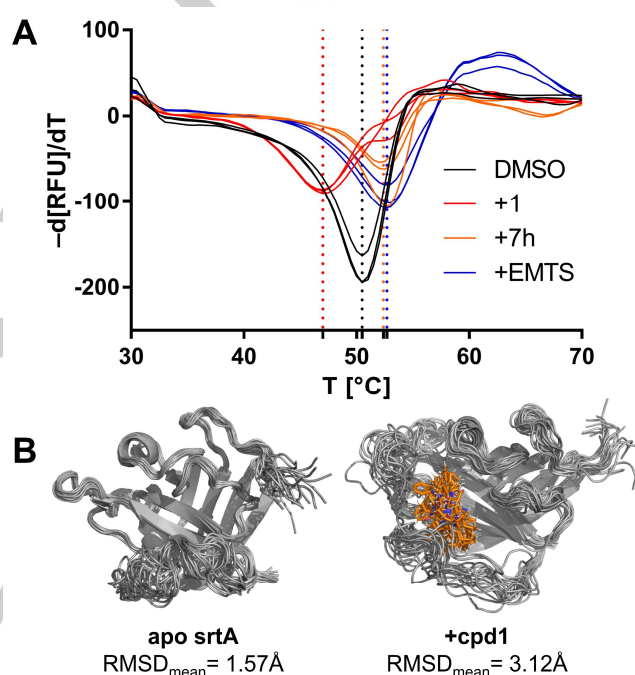

Figure 5. Differential scanning fluorimetry to characterize labeled SrtA proteins. A) Derivative −d(RFU)/dt of the protein denaturing curves to determine the melting temperature (native SrtA: 50.5 °C, +cpd **1**: 47.1 °C, +cpd **7h**: 52.4 °C, +EMTS: 52.7 °C). B) Structural super-positioning of the NMR-structures pdb: 1IJA (apo SrtA) and pdb: 2MLM (+cpd **1**) showing differences in overall disorder.

Molecular modeling of the ligand-binding

Molecular docking studies were performed by FlexX docking within the LeadIT worksuite. The docking of the non-covalently bound inhibitors resulted in a conformation that aligned well with the benzisothiazolinone inhibitor of the NMR-structure pdb: 2MLM (Fig 6). When docked into the active site of SrtA **12a** inserted its space-filling 3-phenoxyaniline moiety into the lipophilic sub-pocket generated by the side chains of Thr122, Ile124 and the hydrophobic stretch of the β6/7-loop (Val108–Leu111). This might explain why altering the 3-phenoxyaniline fragment to smaller or less hydrophobic moieties, such as isobutylamine at the R^1 position, reducing the potency up to threefold. However, the flexible β6/7-loop was previously shown to adapt to

6

substrate/inhibitor binding, and hence, it was difficult to predict the optimal R[1] substituent *ab inito* by molecular modeling.[66]

On the amino acid linker, both the carbonyl oxygen and the aspartic acid side chain group were positioned towards the highly conserved side chain of Arg139, suggesting a potential hydrogen-bonding network. This could explain the observed reduction in activity when non-polar functional groups were introduced to the amino acid position of the inhibitor scaffold. The disulfanylbenzamide aromatic system was enclosed by π-π interactions in a sub-pocket comprising His62, Tyr129 and Trp136 positioning the disulfide warhead towards the targeted Cys126. With *meta* or *para*-substituted inhibitors (**7u** and **7α**), no reasonable docking pose could be generated explaining their low inhibitory activity. Furthermore, we found the alkyl sulfur atom at a distance of 3.53 Å to the Cys126, whereas the aromatic sulfur atom had a distance of 3.90 Å. The closer proximity of the alkyl sulfur atom supported the findings that most likely the thioethyl fragment was transferred. The docking calculations suggested the dithioethyl group to be the largest tolerated R[2] substituent due to the gatekeeping Leu39 residue. Correspondingly, larger alkyl substituents such as *i*Pr, *t*Bu, EtPh led to a substantial decrease in inhibition.
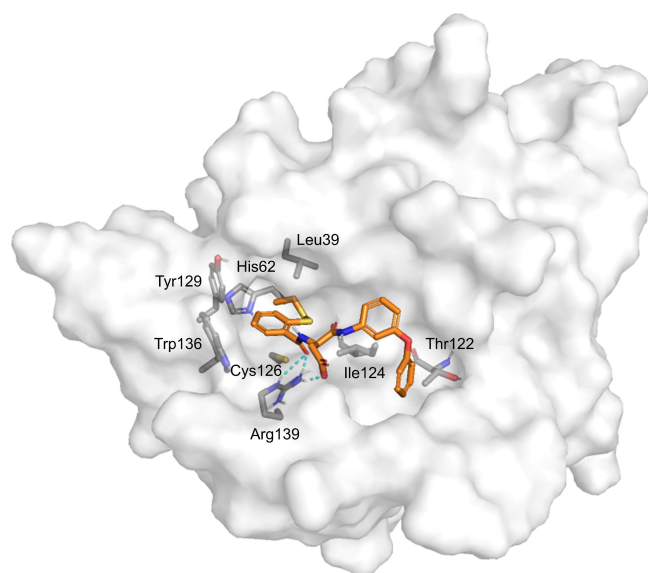

Figure 7. Analysis of fibrinogen-mediated adherence inhibition of *S. aureus* SA113. Different concentration (5 and 10 µM) of the various inhibitors were added to the bacterial inoculum and the biofilm was allowed to form overnight by static grow at 30 °C. The total biofilm was determined. Untreated bacteria served as control. Graphs represent the results of four independent biological replicates. Error bars indicate the mean value with the standard deviation.

Figure 6. Docking pose of inhibitor **12a** in complex with the NMR structure (pdb: 2MLM) highlighting the proposed interaction features upon non-covalent binding.

Effect on fibrinogen-mediated adherence of S. *aureus*

To determine the effect of SrtA inhibitors on living bacterial cells we studied the ability of various *S. aureus* strains to adhere to fibrinogen-coated surfaces, a prerequisite mechanism for biofilm formation and the pathogenesis of bloodstream infections.[67] The treatment of the *S. aureus* SA113 strain with a set of selected disulfanylbenzamides efficiently reduced staphylococcal binding to fibrinogen (Fig 7). Here, we identified compound **7g** as the most potent adherence inhibitor with 66% adherence reduction at a concentration of 10 µM. The mono-maleamide **16b** did not show a significant reduction of adherence. In contrast to the efficient reduction of adherence in SA113 cells, we did not observe significant effects in *S. aureus* USA300 cells at final inhibitor concentrations of 10 µM (data not shown).
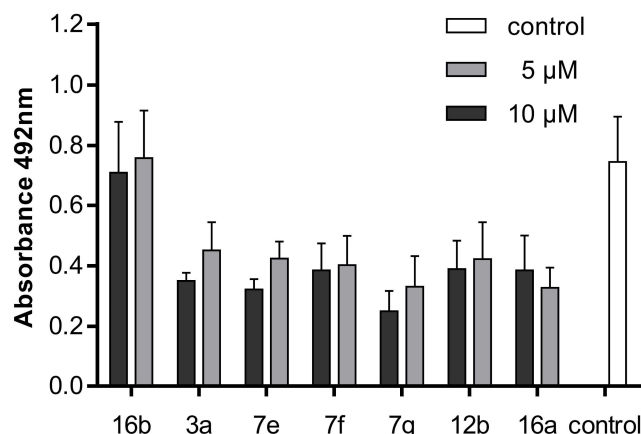
Inhibition of synthetic substrate incorporation in *S. aureus*

The activity of SrtA on the surface of *S. aureus* was determined by employing a fluorescein-conjugate of the LPXTG-substrate (FAM-GSLPETGGS-NH$_2$). When added to the cell culture, the fluorescence label is incorporated into the cell wall, and thus, SrtA activity can be measured by fluorescence quantification.[25,68] **7f** was selected as the model compound because it showed one of the best potencies in both the fluorometric assay and the adherence assays. **7f** inhibited the incorporation of the substrate in a concentration-dependent manner in SA113 cells (Fig 8). For the USA300 strain, however, only weak inhibition (17% at 100 µM of **7f**) was detected, which is in agreement with the results of the fibrinogen adherence assays.

The combined data suggest interesting strain-specific effects of disulfanylbenzamides. Of note, the USA300 strain was described before as less susceptible to SrtA-targeting compounds. Thus, rhodanines (which are known as covalent modifiers of SrtA[30]) were found to be 40-fold weaker biofilm inhibitors in USA300 compared to SA113.[69] Our data suggest that this insusceptibility of USA300 might also hold true for the disulfanylbenzamides tested in this study. The reasons for these differences remain unknown, but it is conceivable that the two strains might differ regarding their overall cell wall composition, and that the inhibitors are therefore unable to reach the SrtA protein in the cell wall of USA300. However, at the present stage the issue needs further investigation.
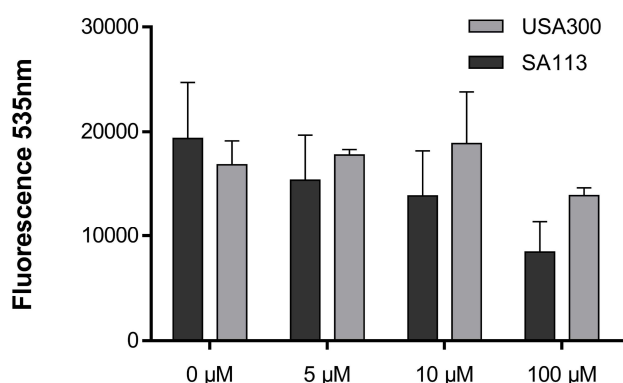
Figure 8. Inhibition of SrtA-mediated incorporation of a synthetic fluorescence substrate into the cell wall of *S. aureus* SA113 and USA300. Different concentrations of compound **7f** (5, 10 and 100 µM) were added to the bacteria inoculum containing 0.3 mM FAM-GSLPETGGS-NH$_2$ and cells were grown overnight. After washing and removal of non-covalently bound FAM-substrate, the fluorescence was measured. Graphs represent the results of three independent biological replicates and error bars indicate the mean with the standard deviation.

Growth inhibition of bacterial cells

To test the bacterial growth inhibition by the compounds, we determined the minimum inhibitory concentration (MIC) by a microbroth dilution assay. The inhibitors which showed effective adherence reduction (**7e**, **7f**, **7g**, **12b**, and **16a**) were tested for growth inhibition in two strains of *S. aureus* (SA113 and USA300) and one *E. coli* strain (Table 3). Unlike parent compound **1**, which rapidly killed *Staphylococci* (MIC=2.92 µM[32]), the addition of most disulfanylbenzamides to staphylococcal cultures had no measurable effect on the growth of *S. aureus* strains at effective adherence inhibition concentrations (5–10 µM).

Table 3. The minimal inhibitory concentration of representative compounds on two strains of *S. aureus* and one *E. coli* strain.

Cpd.	Structure	MIC [µM]		
		SA113	USA300	*E. coli*
7e		16.0	16.0	>500
7f		7.74	15.4	>500
7g		116	464	>500
12b		222	222	>500
16a		381	381	>500

All results include the median value from three biological replicates with two technical replicates each.

While the inhibitors **7e** and **7f** showed medium cell growth inhibition at higher concentrations (MIC=7–16 µM), all other inhibitors did not exhibit any effect at <100 µM. The MIC for all inhibitors tested on *E. coli* was higher than the upper test limit of

200 mg/L, indicating that these compounds only affect Gram-positive bacteria. These results indicate that most disulfanylbenzamides selectively inhibit SrtA activity and do not function as antibiotics for *S. aureus* strains.

Protease inhibition selectivity

Mammalian cathepsin B, L and SrtA are all structurally related to papain-like proteases, thus, we used their relatedness to study the selectivity of our inhibitors.[70] In fact, disulfides and isothiazolinones are known inhibitors of the cathepsin family.[71–73] In line with previous cytotoxicity studies,[74,75] parent compound **1** and the fragment-based inhibitor **3a** showed the weakest selectivity and up to 100% inhibition at 20 µM on both cathepsins (Table 4). However, most disulfanylbenzamides displayed no inhibition of cathepsin L and only moderate inhibition of cathepsin B, indicating a favorable shift of selectivity.

Table 4. Protease inhibition selectivity of a representative compound set. Compounds were tested at a final concentration of 20 µM inhibitor.

Cpd.	structure	inhibition [%] at 20 µM		
		cathepsin B	cathepsin L	NS2B/NS3 (ZIKV)
1		98% ±0.4%	79% ±2.2%	n.i.
3a		100% ±0.5%	93% ±5.6%	n.i.
7a		98% ±0.1%	14% ±8.9%	18% ±1.1%
7f		60% ±0.5%	n.i.	12% ±3.1%
7g		18% ±3.9%	n.i.	17% ±7.7%
7h		69% ±1.7%	23% ±11%	13% ±8.0%
12a		90% ±0.5%	n.i.	15% ±5.7%

n.i.= no inhibition at 20 µM compound concentration. All results include the mean value and standard deviations from triplicate measurements.

As endopeptidases, both cathepsins prefer large hydrophobic amino acids in the P2 site.[76] This might explain why the 3-phenoxyaniline inhibitors (**7a** and **12a**) showed the highest cathepsin inhibition (90–98%) among all disulfanylbenzamides. The exopeptidase activity makes cathepsin B unique among cysteine cathepsins, thus, we hypothesized this could cause the selectivity of our inhibitors within the cathepsin family and might favor the binding of the carboxylic acid **12a** to the histidine-rich occluding loop of cathepsin B.[77] The ZIKV NS2B/NS3 protease is a serine protease and contains only two non-catalytic cysteine residues, thus as expected, only minimal inhibition by all of our thiol-reactive compounds was observed.[78] Compound **7g** showed neither relevant inhibition of cathepsins nor the NS2B/NS3 protease, while it was the most potent inhibitor in the fibrinogen adherence assay on *S. aureus* (Fig 7). This is a

8

FULL PAPER

remarkable improvement compared to the weak selectivity of parent compound **1**.

Cytotoxicity on HeLa cells

In vitro cytotoxicity assessment of disulfanylbenzamides was accomplished on HeLa cells using the MTT-assay. The results demonstrated the non-toxic properties of disulfanylbenzamides at relevant treatment concentrations (Table 5). While the parent compound **1** displayed a CC_{50} of 87 µM, the cytotoxicity of the disulfanylbenzamides was between 156 µM and >1000 µM. (Tables 5).[79]

Table 5. Cytotoxicity (CC_{50}) toward HeLa cells and srtA inhibition constant values (K_i) of representative compounds.

Cpd.	structure	CC_{50} [µM]	K_i [µM]
1		87 ±2.8	34.2 ±5.87
3a		409 ±3.9	367 ±24.4
7e		316 ±31	16.2 ±2.87
7f		156 ±8.5	14.3 ±2.87
7g		253 ±67	17.0 ±3.04
7h		>1000	20.5 ±3.53
7m		>1000	6.40 ±0.84
7o		762 ±137	8.24 ±1.12
12a		331 ±36	10.3 ±2.3

All results include the mean value and standard deviations from triplicate measurements.

Compounds **7f** and **7h** differed only by the *N*-methylation of the amide bond. The affinity (K_i) and reactivity (k_{inact}) of both inhibitors did not deviate significantly, but the methylated substance **7h** showed reduced cytotoxicity by a factor of >8. The metabolic conversion of substituted disulfanylbenzamides to benzisothiazolinones could be a cause for this different cytotoxicity behavior (Scheme 4).[80,81]
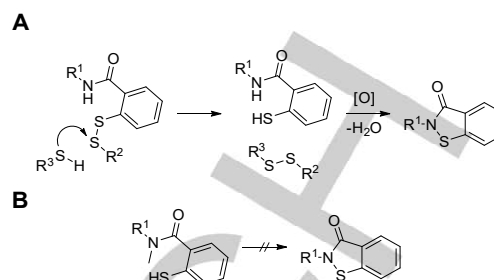
Scheme 4. Hypothesis for a proposed metabolic conversion of disulfanylbenzamides to benzisothiazolinones in adaption to Nikolayevskiy *et al.*[81] A) Transfer of the thioalkyl fragment (R^2) to cellular thiols (R^3) leaves the 2-mercaptobenzamide which can be metabolized to benzisothiazolinones. B) By means of the *N*-methylation, this metabolic conversion is blocked.

In this case, the *N*-methylation of **7h** prevented the conversion to the benzisothiazolinone **1** (Scheme 4b). A recent metabolism study suggested the thermodynamics of 2-sulfanylbenzamides' metabolism having a strong effect on its biological activity.[81] A metabolic involvement is supported by the fact that only prolonged cellular incubation times (48 h) with all disulfanylbenzamides lead to significant cytotoxic effects.

Conclusions

Based on a warhead chemotype transformation strategy, we discovered a novel class of small-molecule SrtA inhibitors. We established the structure-activity relationship of a broad series of substituted disulfanylbenzamides and defined the structural requirements for efficient SrtA inhibition. The choice of a warhead for irreversible inhibitors was guided by the particular biochemical properties of the catalytic Cys126. We concluded from our findings that covalent targeting is much more effective by disulfanylbenzamides than by conventional Michael-acceptor warheads. The pH-independent transfer of a thioethyl fragment (+60.0 Da) was found to be the predominant mode of action for SrtA inhibition. While showing low mammalian cytotoxicity (CC_{50}=253 µM), weak bacterial growth inhibition (MIC=116 µM), and low off-target protease inhibition, compound **7g** was the most effective inhibitor in diminishing *S. aureus* fibrinogen adherence (–66% at 10 µM). Therefore, we concluded that, as a lead structure, compound **7g** should be investigated in further studies. The selectivity differences in adherence inhibition between the *S. aureus* strains SA113 and USA300 should also be addressed in further studies, just as the potential of any bacterial resistance development towards disulfanylbenzamides.

FULL PAPER

Experimental Section

Synthesis: Protocols for the synthesis of all final products and intermediates with their respective analytical data can be found in the SI.

Protein expression and purification: Expression of the *S. aureus* SrtA was performed as described previously.[41] *E. coli* strain BL21-Gold (DE3) cells (Agilent Technologies, Santa Clara, California) were transformed with a pET23b expression construct and grown in LB medium containing 100 µM ampicillin at 37 °C to an OD_{600} of ~0.7. Expression was induced with 1 mM isopropyl-D-thiogalactoside (IPTG) for 16 h at 20 °C. After harvesting, cells were resuspended in lysis buffer (20 mM Tris-HCl, pH 6.9, 300 mM NaCl, 0.1% Triton X-100, RNase, DNase, lysozyme) and lysed by sonication (Sonoplus, Bandelin, Berlin, Germany). The lysate was cleared by centrifugation (45 min at 15 krpm) and the protein was purified from the supernatant by IMAC (HisTrap HP 5 mL column, GE Healthcare, Chicago, Illinois). Eluted proteins were subsequently subjected to a gel-filtration step (HiLoad 16/60 Superdex 200 column, GE Healthcare) and eluted in the storage buffer (20 mM Tris-HCl, pH 7.50, 150 mM NaCl, 5 mM $CaCl_2$). Purified proteins were concentrated, shock frozen in liquid nitrogen and stored at –80 °C until further usage. Throughout all steps, protein concentrations were measured via absorbance at 280 nm and sample purity was assessed via SDS-PAGE.

Inhibition of sortase A: Inhibition of SrtA-catalyzed *in vitro* transpeptidation was performed as described previously.[20,82] Briefly, the recombinantly expressed SrtA (final concentration: 1 µM) was incubated in assay buffer (50 mM Tris, 150 mM NaCl, 5 mM $CaCl_2$, pH 7.50) with 25 µM of the FRET-pair substrate Abz-LPETG-Dap(Dnp)-OH (Genscript, Piscataway, New Jersey) and 0.5 mM tetraglycine (Sigma Aldrich, St. Louis, Missouri). Inhibitors were added from DMSO stocks. Negative inhibition control was performed by mock treatment with DMSO. Reactions were initiated by addition of SrtA and monitored for 30 min at 25 °C in an Infinite M200 Pro plate reader with λ_{ex} 320 nm/λ_{em} 430 nm (Tecan, Männedorf, Switzerland). Three technical replicates were carried out for each inhibitor in black flat-bottom 96-well plates (Greiner bio-one, Kremsmünster, Austria). The enzyme kinetics were analyzed as described previously.[83] To determine first-order inactivation rate constants (k_{obs}) for the irreversible inhibition, progress curves were analyzed by nonlinear regression analysis (t=0–10 min) using the equation: $F = [P]^{\infty}(1 - e^{-k_{obs} \cdot t}) + offset$. Fitting of the k_{obs} values against the inhibitor concentrations to the hyperbolic equation $k_{obs} = (k_{inact} [I])/(K_{Iapp} + [I])$ gave the individual values of K_{Iapp} and k_{inact}. Progress curves and k_{obs} vs [I] plots of all active compounds can be found in the SI figures 5–7. K_{Iapp} values were corrected to the zero-substrate concentration by the Cheng-Prusoff equation $K_i = K_{Iapp}/(1 + \frac{[S]}{K_M})$. For [S]<<$K_M$ we assumed K_{Iapp} = K_i.

Protease inhibition selectivity: Fluorometric assays of the ZIKV NS2B/NS3 protease were performed as described previously.[84] The assay was carried out in triplicates at 25 °C in assay buffer (50 mM Tris, pH 9.0, 20% glycerol and 1 mM CHAPS). 100 µM Boc-GRR-AMC (Bachem, Bubendorf, Switzerland) was used as a substrate on a Tecan Infinite M200 Pro plate reader (λ_{ex} 380 nm/λ_{em} 460 nm). Fluorometric assays for cathepsin B and cathepsin L (Calbiochem, Merck Millipore, Burlington, Massachusetts) were performed as described previously.[85] Cbz-Phe-Arg-AMC was used as substrate (80 µM for cathepsin B, 5 µM for cathepsin L) in assay buffer (20 mM Tris, pH 6.0, 5 mM EDTA, 200 mM NaCl, 0.005% Brij).

Protein mass spectrometry: An *S. aureus* SrtA stock solution (3.8 µL, 760 µM) was diluted in 500 µL enzyme dilution buffer (50 mM Tris, 150 mM NaCl, 5 mM $CaCl_2$, pH 7.50). The compounds **7h** and **16b** were dissolved in DMSO to generate stock solutions. Inhibitors were added to SrtA at a final concentration of 400 µM and were allowed to react for 1 h at room temperature. Samples were stored until MS analysis at –20 °C. The detailed procedure for the proteolytic digestion and the LC/MS can be found in the SI.

Differential scanning fluorimetry: Thermal shift assays were conducted in triplicate using a C1000/CFX384 qPCR system (Bio-Rad, Hercules, California) using the FRET channel and contained SrtA (2.2 µg), the respective test compound (50 µM) and Sypro Orange (5×) in 25 µL of assay buffer (50 mM Tris, 150 mM NaCl, 5 mM $CaCl_2$, pH 7.50). The samples were heated at 0.5 °C/s, from 25 to 75 °C. The fluorescence intensity was plotted as a function of the temperature. The melting point was given by the inflection point of the fluorescence curve as calculated by the High-Precision-Melt software (Bio-Rad).

Cell viability assay (HeLa Cells): Cell culturing was performed in a humidified incubator at 37 °C with 5% CO_2 atmosphere. HeLa cells were grown in cell culture flasks according to standard protocols (Dulbecco's Modified Eagle Medium [DMEM], 10% (v/v) fetal calf serum, 1% pyruvate, and 1% penicillin-streptomycin) and seeded to 96-well microplates at a concentration of 15,000 cells in a volume of 100 µL of DMEM. Inhibitors were dissolved at a concentration of 7.8–250 µg/mL in DMEM containing DMSO (0.08%–2.5%) and added in triplicates to the HeLa cells. Negative inhibition control was performed by mock treatment with DMEM with DMSO in the same concentration as the compound solutions were used. After an incubation time of 48 h (37 °C, 5% CO_2) a solution of 3-(4,5-dimethyl-2-thiazolyl)-2,5-diphenyl-2*H*-tetrazolium bromide (MTT) in DMEM (40 µL, 3.0 mg/mL) was added directly to each well and the plate was incubated for additional 20 min. The medium was aspirated and replaced by 200 µL of DMSO and 25 µL of glycine buffer (0.1 M glycine, 0.1 M NaCl, pH 10.5). After shaking for 20 min, the absorbance was measured at 595 nm using an Infinite M200 Pro plate reader (Tecan). The background at 670 nm and the absorbance of the compounds at the same wavelength was subtracted from the data obtained from the first readout. Cell viability was normalized to the absorbance measured from DMSO-DMEM threated cells.

Bacterial growth inhibition: The MIC of different inhibitors was determined against *S. aureus* USA300[86], SA113[87] and a laboratory strain of *E. coli* using the microbroth dilution assay according to standard protocols in 96-well, polystyrene tissue culture plates (Greiner Bio-One, Cellstar, F-form). The MIC was determined as the concentration of the inhibitor where the lowest OD_{595} values were recorded with a Tecan Infinite 200Pro (Tecan).

***S. aureus* adherence assay:** *S. aureus* adherence was tested in 96-well, polystyrene tissue culture plates (Greiner Bio-One, Cellstar, F-form) as previously described[88] with the following modifications. Before starting the experiment, the plates were coated with fibrinogen.[89] Fibrinogen from human plasma (Sigma Aldrich) was dissolved in NaCl solution (0.9%) to 10 mg/mL. A fibrinogen solution of 100 µg/mL was prepared in PBS and 100 µL were dispensed into each well of the plate. After sealing, the plate was incubated at 4 °C overnight to allow fibrinogen coating of the well. The next day, the fibrinogen solution was aspirated. Bacterial strains (OD_{600}~0.05 in tryptic soy broth) were incubated under static conditions in the presence of different dilutions of inhibitors in 1.6% DMSO at 30 °C for 18 h. The next day, the planktonic bacteria were discarded, the plates were rinsed twice with PBS (1×) and the biofilm was heat-fixed at 65 °C for 1 h. Plates were stained with 10 mg/mL crystal violet for 2 min, washed twice with double-distilled water before measuring the absorbance at OD_{492} with an ELISA plate reader (Multiskan Ascent, Thermo Fisher Scientific, Waltham, Massachusetts).

Incorporation of synthetic SrtA substrates on *S. aureus*: The FAM-GSLPETGGS-NH_2 substrate was synthesized using a 3D-printed solid-phase peptide synthesizer[90] (detailed procedure in the SI). The incorporation of a synthetic substrate on the *S. aureus* cell wall was conducted as described previously with minor modifications.[25] USA300 and SA113 were grown in tryptic soy broth medium in the presence of 0.3 mM FAM-GSLPETGGS-NH_2 and different concentrations of compound **7f**. After 15 h, cells (OD_{600}~8) were harvested from all cultures in a final volume of 500 µL and washed with cold PBS (1×). Non-covalently bound substrate was removed by treatment with 5% SDS for 5 min at

10

FULL PAPER

60 °C. Cells were washed twice with cold PBS and then suspended in 200 µL PBS. The fluorescence of incorporated substrate was measured with an Infinite M200 Pro plate reader (λ_{ex} 485 nm/λ_{em} 535 nm).

Molecular modeling: A FlexX-algorithm docking protocol was conducted within the LeadIT-2.3.2 worksuite.[91] The NMR-structure 2MLM (frame 18) was downloaded from the Protein Databank (pdb). Prior to docking, the benzisothiazolinone-modified active-site Cys126 was untethered and reprotonated with MOE2019.01.[92] Receptor preparation was performed using the automated binding site and protonation detection routine within LeadIT. Ligands were energy minimized using the MMFF94 force field within MOE. The docking protocol was performed under default parameters using the hybrid approach (enthalpy/entropy) for ligand placement.

Acknowledgments

Keywords: Antibiotics • Biofilm • Drug design • Sortase A • *Staphylococcus aureus*
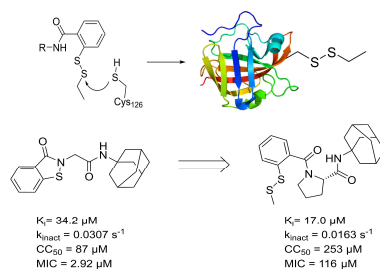
References:

[1] S. W. Dickey, G. Y. C. Cheung, M. Otto, *Nat. Rev. Drug. Discov.* **2017**, *16*, 457–471.

[2] G. Michaud, R. Visini, M. Bergmann, G. Salerno, R. Bosco, E. Gillon, B. Richichi, C. Nativi, A. Imberty, A. Stocker, et al., *Chem. Sci.* **2016**, *7*, 166–182.

[3] W. J. Weiss, E. Lenoy, T. Murphy, L. Tardio, P. Burgio, S. J. Projan, O. Schneewind, L. Alksne, *J. Antimicrob. Chemother.* **2004**, *53*, 480–486.

[4] S. K. Mazmanian, G. Liu, E. R. Jensen, E. Lenoy, O. Schneewind, *Proc. Natl. Acad. Sci.* **2000**, *97*, 5510–5515.

[5] A. W. Maresso, O. Schneewind, *Pharmacol. Rev.* **2008**, *60*, 128–141.

[6] S. K. Mazmanian, G. Liu, H. Ton-That, O. Schneewind, *Science* **1999**, *285*, 760–763.

[7] J. Zhang, H. Liu, K. Zhu, S. Gong, S. Dramsi, Y.-T. Wang, J. Li, F. Chen, R. Zhang, L. Zhou, et al., *Proc. Natl. Acad. Sci.* **2014**, *111*, 13517–13522.

[8] S. Cascioferro, M. Totsika, D. Schillaci, *Microb. Pathog.* **2014**, *77*, 105–112.

[9] D. Mu, H. Xiang, H. Dong, D. Wang, T. Wang, *J. Microbiol. Biotechnol.* **2018**, *28*, 7.

[10] W. W. Navarre, O. Schneewind, *Microbiol. Mol. Biol. Rev.* **1999**, *63*, 174–229.

[11] N. Suree, C. K. Liew, V. A. Villareal, W. Thieu, E. A. Fadeev, J. J. Clemens, M. E. Jung, R. T. Clubb, *J. Biol. Chem.* **2009**, *284*, 24465–24477.

[12] A. M. Perry, H. Ton-That, S. K. Mazmanian, O. Schneewind, *J. Biol. Chem.* **2002**, *277*, 16241–16248.

[13] E. Tsompanidou, E. L. Denham, M. J. J. B. Sibbald, X. Yang, J. Seinen, A. W. Friedrich, G. Buist, J. M. van Dijl, *PLoS One* **2012**, *7*, e44646.

[14] O. Schneewind, D. Missiakas, *Protein Secretion Pathways Bact.* **2019**, 173–188.

[15] K. W. Clancy, J. A. Melvin, D. G. McCafferty, *Pept. Sci.* **2010**, *94*, 385–396.

[16] U. Ilangovan, H. Ton-That, J. Iwahara, O. Schneewind, R. T. Clubb, *Proc. Natl. Acad. Sci.* **2001**, *98*, 6056–6061.

[17] W. van 't Hof, S. H. Maňásková, E. C. I. Veerman, J. G. M. Bolscher, *Biol. Chem.* **2015**, *396*, 283–293.

[18] K. Kappel, J. Wereszczynski, R. T. Clubb, J. A. McCammon, *Protein Sci.* **2012**, *21*, 1858–1871.

[19] J. Zhu, L. Xiang, F. Jiang, Z. J. Zhang, *Exp. Biol. Med. (Maywood)* **2016**, *241*, 90–100.

[20] R. G. Kruger, P. Dostal, D. G. McCafferty, *Anal. Biochem.* **2004**, *326*, 42–48.

[21] J. A. Melvin, C. F. Murphy, L. G. Dubois, J. W. Thompson, M. A. Moseley, D. G. McCafferty, *Biochemistry* **2011**, *50*, 7591–7599.

[22] B. C. Chenna, J. R. King, B. A. Shinkre, A. L. Glover, A. L. Lucius, S. E. Velu, *Eur. J. Med. Chem.* **2010**, *45*, 3752–3761.

[23] P. M. Wehrli, I. Uzelac, T. Olsson, T. Jacso, D. Tietze, J. Gottfries, *Bioorg. Med. Chem.* **2019**, 115043.

[24] S. Oniga, C. Araniciu, M. Palage, M. Popa, M.-C. Chifiriuc, G. Marc, A. Pirnau, C. Stoica, I. Lagoudis, T. Dragoumis, et al., *Molecules* **2017**, *22*, 1827.

[25] I. Rentero Rebollo, S. McCallin, D. Bertoldo, J. M. Entenza, P. Moreillon, C. Heinis, *ACS Med. Chem. Lett.* **2016**, *7*, 606–611.

[26] Y. Zhang, J. Bao, X.-X. Deng, W. He, J.-J. Fan, F.-Q. Jiang, L. Fu, *Bioorg. Med. Chem. Lett.* **2016**, *26*, 4081–4085.

[27] S. Cascioferro, D. Raffa, B. Maggio, M. V. Raimondi, D. Schillaci, G. Daidone, *J. Med. Chem.* **2015**, *58*, 9108–9123.

[28] G. Nitulescu, A. Zanfirescu, O. T. Olaru, I. M. Nicorescu, G. M. Nitulescu, D. Margina, *Molecules* **2016**, *21*, 1591.

[29] A. W. Maresso, R. Wu, J. W. Kern, R. Zhang, D. Janik, D. M. Missiakas, M.-E. Duban, A. Joachimiak, O. Schneewind, *J. Biol. Chem.* **2007**, *282*, 23129–23139.

[30] N. Suree, S. W. Yi, W. Thieu, M. Marohn, R. Damoiseaux, A. Chan, M. E. Jung, R. T. Clubb, *Bioorg. Med. Chem.* **2009**, *17*, 7174–7185.

[31] A. H. Chan, S. W. Yi, E. M. Weiner, B. R. Amer, C. K. Sue, J. Wereszczynski, C. A. Dillen, S. Senese, J. Z. Torres, J. A. McCammon, et al., *Chem. Biol. Drug Des.* **2017**, *90*, 327–344.

[32] D. Zhulenkovs, Z. Rudevica, K. Jaudzems, M. Turks, A. Leonchiks, *Bioorg. Med. Chem.* **2014**, *22*, 5988–6003.

[33] K. Jaudzems, V. Kurbatska, A. Jēkabsons, R. Bobrovs, Z. Rudevica, A. Leonciks, *ACS Infect. Dis.* **2019**, acsinfecdis.9b00265.

[34] G. Nitulescu, D. P. Mihai, I. M. Nicorescu, O. T. Olaru, A. Ungurianu, A. Zanfirescu, G. M. Nitulescu, D. Margina, *Drug Dev. Res.* **2019**, ddr.21599.

[35] B. Evans, E. Shaw, *J. Biol. Chem.* **1983**, *258*, 10227–10232.

[36] T. Waag, C. Gelhaus, J. Rath, A. Stich, M. Leippe, T. Schirmeister, *Bioorg. Med. Chem. Lett.* **2010**, *20*, 5541–5543.

[37] C. S. I. Nobel, M. Kimland, D. W. Nicholson, S. Orrenius, A. F. G. Slater, *Chem. Res. Toxicol.* **1997**, *10*, 1319–1324.

[38] F. Yang, W. Wang, K. Li, W. Zhao, X. Dong, *Tetrahedron Lett.* **2017**, *58*, 218–222.

[39] S. Kusaka, R. Matsuda, S. Kitagawa, *Chem. Commun.* **2018**, *54*, 4782–4785.

[40] M. R. James, *Process for the Preparation of 1,2-Benzisothiazolin-3-Ones*, **2004**, KR100429082B1.

[41] L. Schmohl, J. Bierlmeier, F. Gerth, C. Freund, D. Schwarzer, *J. Pept. Sci.* **2017**, *23*, 631–635.

[42] B.-F. Krippendorff, R. Neuhaus, P. Lienau, A. Reichel, W. Huisinga, *J. Biomol. Screening* **2009**, *14*, 913–923.

[43] J. M. Strelow, *SLAS Discovery* **2017**, *22*, 3–20.

[44] M. Gehringer, S. A. Laufer, *J. Med. Chem.* **2019**, *62*, 5673–5724.

[45] J. B. Baell, J. W. M. Nissink, *ACS Chem. Biol.* **2018**, *13*, 36–44.

[46] C. J. Scott, A. McDowell, S. L. Martin, J. F. Lynas, K. Vandenbroeck, B. Walker, *Biochem. J.* **2002**, *366*, 953–958.

[47] K. M. Connolly, B. T. Smith, R. Pilpa, U. Ilangovan, M. E. Jung, R. T. Clubb, *J. Biol. Chem.* **2003**, *278*, 34061–34065.

[48] B. A. Frankel, R. G. Kruger, D. E. Robinson, N. L. Kelleher, D. G. McCafferty, *Biochemistry* **2005**, *44*, 11188–11200.

[49] A. C. C. Plette, W. H. van Riemsdijk, M. F. Benedetti, A. van der Wal, *J. Colloid Interface Sci.* **1995**, *173*, 354–363.

[50] P. D. Cotter, C. Hill, *Microbiol. Mol. Biol. Rev.* **2003**, *67*, 429–453.

[51] L. Schmohl, F. R. Wagner, M. Schümann, E. Krause, D. Schwarzer, *Bioorg. Med. Chem.* **2015**, *23*, 2883–2889.

[52] I. Klimenkovs, E. Bakis, A. Priksane, *Synth. Commun.* **2013**, *43*, 2634–2640.

[53] U. Bhatt, B. C. Duffy, P. R. Guzzo, L. Cheng, T. Elebring, *Synth. Commun.* **2007**, *37*, 2793–2806.

11

[54]   H. Feuer, E. H. White, J. E. Wyman, *J. Am. Chem. Soc.* **1958**, *80*, 3790–3792.

[55]   A. Paasche, A. Zipper, S. Schäfer, J. Ziebuhr, T. Schirmeister, B. Engels, *Biochemistry* **2014**, *53*, 5930–5946.

[56]   R. D. Bach, O. Dmitrenko, C. Thorpe, *J. Org. Chem.* **2008**, *73*, 12–21.

[57]   R. E. Benesch, R. Benesch, *J. Am. Chem. Soc.* **1958**, *80*, 1666–1669.

[58]   G. I. Giles, C. Jacob, *Biological Chemistry* **2002**, *383*, 375–388.

[59]   A. P. Ryle, F. Sanger, *Biochem. J.* **1955**, *60*, 535–540.

[60]   P. Nagy, *Antioxid. Redox. Signal.* **2013**, *18*, 1623–1641.

[61]   R. Alvarez-Sánchez, D. Basketter, C. Pease, J.-P. Lepoittevin, *Bioorg. Med. Chem. Lett.* **2004**, *14*, 365–368.

[62]   M.-A. Morren, A. Dooms-Goossens, J. Delabie, C. D. Wolf-Peeters, K. Marien, H. Degreef, *Dermatology* **1992**, *184*, 260–264.

[63]   B. M. Dorr, H. O. Ham, C. An, E. L. Chaikof, D. R. Liu, *Proc. Natl. Acad. Sci.* **2014**, 201411179.

[64]   D. J. Smith, E. T. Miggio, G. L. Kenyon, *Biochemistry* **1975**, *14*, 766–771.

[65]   Y. Zong, S. K. Mazmanian, O. Schneewind, S. V. L. Narayana, *Structure* **2004**, *12*, 105–112.

[66]   C. Gao, I. Uzelac, J. Gottfries, L. A. Eriksson, *Sci. Rep.* **2016**, *6*, 20413.

[67]   M. McAdow, H. K. Kim, A. C. DeDent, A. P. A. Hendrickx, O. Schneewind, D. M. Missiakas, *PLoS Pathog.* **2011**, *7*, e1002307.

[68]   S. H. Maňásková, K. Nazmi, W. van 't Hof, A. van Belkum, N. I. Martin, F. J. Bikker, W. J. B. van Wamel, E. C. I. Veerman, *PLoS One* **2016**, *11*, e0147401.

[69]   T. J. Opperman, S. M. Kwasny, J. D. Williams, A. R. Khan, N. P. Peet, D. T. Moir, T. L. Bowlin, *Antimicrob. Agents Chemother.* **2009**, *53*, 4357–4367.

[70]   W. J. Bradshaw, A. H. Davies, C. J. Chambers, A. K. Roberts, C. C. Shone, K. R. Acharya, *FEBS J.* **2015**, *282*, 2097–2114.

[71]   T. Bratkovič, M. Lunder, T. Popovič, S. Kreft, B. Turk, B. Štrukelj, U. Urleb, *Biochem. Biophys. Res. Commun.* **2005**, *332*, 897–903.

[72]   R. Wisastra, M. Ghizzoni, H. Maarsingh, A. J. Minnaard, H. J. Haisma, F. J. Dekker, *Org. Biomol. Chem.* **2011**, *9*, 1817–1822.

[73]   C. L. Cywin, R. A. Firestone, D. W. McNeil, C. A. Grygon, K. M. Crane, D. M. White, P. R. Kinkade, J. L. Hopkins, W. Davidson, M. E. Labadia, et al., *Bioorg. Med. Chem.* **2003**, *11*, 733–740.

[74]   K. Hu, H.-R. Li, R.-J. Ou, C.-Z. Li, X.-L. Yang, *Environmental Toxicology and Pharmacology* **2014**, *37*, 529–535.

[75]   E. Turos, K. D. Revell, P. Ramaraju, D. A. Gergeres, K. Greenhalgh, A. Young, N. Sathyanarayan, S. Dickey, D. Lim, M. M. Alhamadsheh, *Bioorg. Med. Chem.* **2008**, *16*, 6501–6508.

[76]   Y. Choe, F. Leonetti, D. C. Greenbaum, F. Lecaille, M. Bogyo, D. Brömme, J. A. Ellman, C. S. Craik, *J. Biol. Chem.* **2006**, *281*, 12824–12832.

[77]   M. H. S. Cezari, L. Puzer, M. A. Juliano, A. K. Carmona, L. Juliano, *Biochem. J.* **2002**, *368*, 365–369.

[78]   Y. Li, W. W. Phoo, Y. R. Loh, Z. Zhang, E. Y. Ng, W. Wang, T. H. Keller, D. Luo, C. Kang, *FEBS Lett.* **2017**, *591*, 2338–2347.

[79]   W. G. E. J. Schoonen, W. M. A. Westerink, J. A. D. M. de Roos, E. Débiton, *Toxicol. In Vitro* **2005**, *19*, 505–516.

[80]   P. J. Tummino, P. J. Harvey, T. McQuade, J. Domagala, R. Gogliotti, J. Sanchez, Y. Song, D. Hupe, *Antimicrob. Agents Chemother.* **1997**, *41*, 394–400.

[81]   H. Nikolayevskiy, M. Robello, M. T. Scerba, E. H. Pasternak, M. Saha, T. L. Hartman, C. A. Buchholz, R. W. Buckheit, S. R. Durell, D. H. Appella, *Eur. J. Med. Chem.* **2019**, *178*, 818–837.

[82]   L. Schmohl, J. Bierlmeier, N. von Kügelgen, L. Kurz, P. Reis, F. Barthels, P. Mach, M. Schutkowski, C. Freund, D. Schwarzer, *Bioorg. Med. Chem.* **2017**, *25*, 5002–5007.

[83]   T. Schirmeister, J. Kesselring, S. Jung, T. H. Schneider, A. Weickert, J. Becker, W. Lee, D. Bamberger, P. R. Wich, U. Distler, et al., *J. Am. Chem. Soc.* **2016**, *138*, 8332–8335.

[84]   F. von Hammerstein, L. M. Lauth, S. Hammerschmidt, A. Wagner, T. Schirmeister, U. A. Hellmich, *FEBS Lett.* **2019**, *593*, 2204–2213.

[85]   R. Ettari, E. Nizi, M. E. Di Francesco, M.-A. Dude, G. Pradel, R. Vičík, T. Schirmeister, N. Micale, S. Grasso, M. Zappalà, *J. Med. Chem.* **2008**, *51*, 988–996.

[86]   B. A. Diep, S. R. Gill, R. F. Chang, T. H. Phan, J. H. Chen, M. G. Davidson, F. Lin, J. Lin, H. A. Carleton, E. F. Mongodin, et al., *Lancet* **2006**, *367*, 9.

[87]   S. Iordanescu, M. Surdeanu, *Microbiology* **1976**, *96*, 277–281.

[88]   M. F. Lerch, S. M. Schoenfelder, G. Marincola, F. D. Wencker, M. Eckart, K. U. Förstner, C. M. Sharma, K. M. Thormann, M. Kucklick, S. Engelmann, *Mol. Microbiol.* **2019**, *111*, 1571–1591.

[89]   C. Colomer-Winter, J. A. Lemos, A. L. Flores-Mireles, *Bio-Protoc.* **2019**, *9*.

[90]   F. Barthels, U. Barthels, M. Schwickert, T. Schirmeister, *SLAS Technol.* **2019**, 2472630319877374.

[91]   B. Kramer, M. Rarey, T. Lengauer, *Proteins: Struct., Funct., Bioinf.* **1999**, *37*, 228–241.

[92]   V. MOE, *Quebec: Montreal* **2006**.

WILEY-VCH

FULL PAPER

Entry for the Table of Contents

K_i = 34.2 µM
k_{inact} = 0.0307 s^{-1}
CC_{50} = 87 µM
MIC = 2.92 µM

K_i = 17.0 µM
k_{inact} = 0.0163 s^{-1}
CC_{50} = 253 µM
MIC = 116 µM

Benzisothiazolinone to disulfanylbenzamide warhead chemotype transformation and systematic activity relationship uncovered novel *S. aureus* sortase A inhibitors with potent inhibition of fibrinogen attachment. The transfer of a thioalkyl fragment to the Cys126 was identified as the mode of action. Warhead reactivity fine-tuning yielded inhibitors with selectivity over other cysteine proteases.